ELSEVIER

Contents lists available at ScienceDirect

# Materials Science & Engineering B

journal homepage: www.elsevier.com/locate/mseb





# Lithiophilic current collector based on nitrogen doped carbon nanotubes and three-dimensional graphene for long-life lithium metal batteries

Yanbo Fang <sup>a,1</sup>, Yu-Yun Hsieh <sup>a,1</sup>, Mahnoosh Khosravifar <sup>a</sup>, Kevin Johnson <sup>b</sup>, Paa Kwasi Adusei <sup>a</sup>, Sathya Narayan Kanakaraj <sup>a</sup>, Sarah Preisler <sup>b</sup>, Guangqi Zhang <sup>a</sup>, Vesselin Shanov <sup>a,b,\*</sup>

#### ARTICLE INFO

Keywords: Lithiophilic current collector Lithium metal anodes Lithium-sulfur battery Nitrogen-doped CNT 3D graphene

#### ABSTRACT

Lithium metal as an attractive anode material has been widely used in advanced energy storage devices. However, drawbacks such as growth of lithium dendrites, significant volume changes during the cycling process, causing safety hazards and limited span-life, have impeded the commercial application of lithium metal anode. Here, we present a new composite structure, consisting of porous three-dimensional graphene (3DG) decorated with nitrogen-doped carbon nanotubes (NCNT). The created NCNT-3DG carbon scaffold is resilient towards significant volumetric change during cycling, while the NCNTs serve as lithiophilic sites for uniform lithium nucleation which enables uniform lithium deposition. This novel hybrid endows the lithium anode with a long-term stability reaching up to 1200 cycles at high current density of 10 mA cm<sup>-2</sup>. This significantly improved the performance of the created lithium-sulfur full cells. The demonstrated performance of the NCNT-3DG structure provides new insights for the designing and fabrication of metallic lithium anodes.

## 1. Introduction

Lithium ion batteries (LIBs) are the most common power sources for consumer electronics as well as for electric vehicles and medical devices. However, the conventional LIBs using graphite anode cannot fulfill today's demanding applications, due to their low theoretical capacities [1,2]. More recently, lithium metal anodes-based lithium-air batteries and lithium-sulfur batteries (LSBs) have attracted great attention because of their higher specific capacities compared to the existing LIBs [1.3–6]. Despite their existence for half a century, lithium metal batteries have been restricted for the past several decades because of the formation of lithium dendrites and uncontrollable interfacial chemical reactivity [7,8]. The growth of lithium dendrites due to non-uniform lithium plating/stripping causes failure and safety hazards such as overheating and fire. The high chemical reactivity between lithium metal and electrolyte leads to the formation of solid electrolyte interphase (SEI) [9]. The SEI layer is known with its poor stability during electrochemical cycling of lithium metal that causes its large volume change and unpredictable deposition. Cracking in the SEI layer exposes again fresh lithium to the electrolyte, forming additional SEI. This

repeatedly consumes lithium and electrolyte and therefore causes severe capacity decay and low efficiency [9-12].

In the past few decades, a lot of research has been devoted to overcoming these issues, and the associated research can be classified into four categories, such as: (1) employing solid electrolytes to suppress dendrite penetration [13-15], (2) adjusting the composition of electrolyte or adding additives to the liquid electrolyte to strengthen SEI [16-20], (3) constructing a stable, ion-permeable interfacial layer for Li metal anodes [21–27], and (4) creating a 3D matrix for hosting lithium [28–36]. The first three approaches are effective to some extent for enhancing SEI stability and restraining dendrite formation. However, they are limited to prevent the apparent volume fluctuation of lithium metal during cycling, which is critical for practical applications of Li anodes [37]. In addition, the liquid electrolyte additives used for SEI stabilization would be gradually exhausted during battery cycling [38]. Likewise, solid electrolytes often exhibit low ionic conductivity at room temperature and a large interfacial resistance resulting in unsatisfactory performance [13,14]. The strategy that uses pre-stored Li 3D structured anodes shows attractive properties that impact the behavior of Li nucleation, especially in the initial lithiation period, which will

<sup>&</sup>lt;sup>a</sup> Department of Mechanical and Materials Engineering, University of Cincinnati, Cincinnati, OH 45221-0072, USA

<sup>&</sup>lt;sup>b</sup> Department of Chemical and Environmental Engineering, University of Cincinnati, OH 45221-0012, USA

<sup>\*</sup> Corresponding author at: Department of Mechanical and Materials Engineering, University of Cincinnati, Cincinnati, OH 45221-0072, USA. *E-mail address:* shanovyn@ucmail.uc.edu (V. Shanov).

 $<sup>^{1}</sup>$  These authors contribute equally to this work.

eventually determine the morphology of the plated Li [39]. The porous 3D scaffold reduced volume variation and lowered effective current density associated with increasing the active Li surface. Therefore, porous metal structures such as 3D Cu and Ni have been employed as effective hosts for lithium metal [28,30,31,34]. However, the intrinsic issue of Cu and Ni structures is their high density (~8.9 g cm<sup>-3</sup>) compared to Li (0.53 g cm<sup>-3</sup>), which dramatically lowers the gravimetric energy density of the battery. 3D porous carbon nanostructures, including carbonized wood, carbon nanotube sponges, and graphene based materials have been investigated as efficient lightweight host materials for constructing better lithium metal anodes, due to their good conductivity, excellent chemical and mechanical stability [29,32,35,36,40-45,63]. Although 3D carbon scaffolds have shown promising performances as lithium metal host materials, deposition of Li on carbon needs extra nucleation overpotential due to its lithiaphobicity. Li without enough driving force to deposit, prefers to directly plate on the surface of carbon matrix rather than to fill in the pores, thus not taking advantage of the large internal surface area [46,47]. Therefore, the strategies of 3D scaffold coupled with lithiophilic materials such as nitrogen or oxygen functionalized materials [41,47–50], metals [46,51,52] and silicon [53,54] nanocomposite, have become a new trend.

Herein, we propose a 3D graphene matrix decorated by NCNTs, thus forming a hybrid host material for long lifetime and dendrite-free Li metal anode, which can perform at high current density and high areal capacity loadings. The NCNT-3DG hybrid host could greatly suppress the lithium dendrite formation because of its unique structural and chemical properties. The high specific surface area of the hybrid host can lower the local effective current density to form a uniform Li-ion flux thus reducing the Li dendrite growth [39,45]. The 3DG specifically offers a robust carbon matrix to minimize the volume changes of Li metal electrodes and also a porous scaffold for uniform NCNT growth. NCNTs with in situ nitrogen doping, as suggested here, have been reported as lithiophilic due to the nitrogen functional groups [39,47,50]. Therefore, uniformly distributed NCNTs on 3DG will act as seeds and will guide homogeneous lithium nucleation with small nucleation overpotential. A further homogeneous lithium growth will suppress dendritic lithium formation. In this work we select NCNT-3DG hybrid carbon scaffold to prove it as a superior alternative to traditional host-less lithium metal anodes for constructing lightweight, high current density, dendrite-free lithium metal anodes.

## 2. Experimental section

# 2.1. Synthesis of nitrogen doped carbon nanotubes-three-dimensional graphene (NCNT-3DG) hybrid structure

The synthesis process of the NCNT-3DG hybrid structure has been described in our publication [55]. High quality (sp<sup>2</sup>-domain) 3DG was synthesized through a chemical vapor deposition (CVD) process, which was published previously by our group [56]. Polystyrene (Sigma Aldrich, 210000 M.W.) of 5.5 g, plasticizer diethylene glycol dibenzoate (DEGD, Sigma Aldrich) (1.75 mL) and 40 g nickel powder were mixed in 20 mL toluene to make a nickel powder/polymer thin film as a CVD catalyst precursor for the synthesis of 3DG. The obtained graphene was then used as the substrate to synthesize nitrogen doped (sp<sup>3</sup>-defective) CNTs. NiCo<sub>2</sub>O<sub>4</sub> flake-like nanostructures and acetonitrile (C<sub>2</sub>H<sub>3</sub>N) were used as catalyst and precursor, respectively, for CVD synthesis of nitrogen doped CNTs at 780 °C. The NiCo<sub>2</sub>O<sub>4</sub> nanoflakes were anchored on the 3DG by annealing in air of nickel-cobalt binary hydroxide (NiCoOH) which was synthesized through a solvothermal process. Ni (NO<sub>3</sub>)<sub>2</sub> ·6H<sub>2</sub>O of 0.6 mmol, Co(NO<sub>3</sub>)<sub>2</sub> ·6H<sub>2</sub>O of 1.2 mmol, and urea of 1.8 mmol were dissolved in 40 mL ethanol-aqueous solution (ethanol:DI water = 1:1). The 3DG was immersed in this solution and then treated in a Teflon-lined stainless-steel autoclave at 126 °C for 3 h which yielded the NiCoOH compounds. After this, the 3DG with NiCoOH were

annealed in air at 350 °C for 5 min which caused transformation of NiCoOH to NiCo<sub>2</sub>O<sub>4</sub> nanoflakes. The NiCo<sub>2</sub>O<sub>4</sub>-3DG composite was heated up to 780 °C in a CVD reactor (FirstNano, ET1000) under Ar (1000 sccm). Then, 100 sccm of C<sub>2</sub>H<sub>3</sub>N was introduced for 60 min. Then, the sample was cooled to room temperature at a rate of  $\sim 100~^{\circ}\text{C min}^{-1}$  under Ar (1000 sccm). The last preparation step included etching out nickel and cobalt catalyst with 3 M HCl at 60 °C for 12 h which resulted in formation of NCNT-3DG hybrid structure. The latter was rinsed with DI water to remove the residual acid.

#### 2.2. Materials characterization

The morphology of the obtain materials was observed by scanning electron microscopy (SEM) (FEI XL30, 5-10 kV). Li foil and NCNT-3DG host materials with lithium deposition were rinsed with 1,3-dioxolane to remove the Li salts on the anode surface prior to the SEM investigation. Raman spectroscopy (Renishaw inVia, excited by a 514 nm Ar-ion laser with a laser spot size of  $\sim 1~\mu m2)$  and TEM (FEI CM20, 300 kV) were used to characterize the 3DG and NCNT-3DG. X-ray Photoelec- tron Spectroscopy (XPS) data were obtained via a VG Thermo Scientific MultiLab 3000 ultra-high vacuum surface analysis system, with  $\sim \! \! 10^{-9}$ Torr base pressure using an Al  $K\alpha$  source of 1486.6 eV excitation energy. The XPS high-resolution scans for carbon and low-resolution survey scans were taken for each sample on at least two different locations. Brunauer-Emmett-Teller (BET) surface area analysis, nitrogen adsorption-desorption isotherm and Density-Function-Theory (DFT) pore size distribution study of 3DG and NCNT-3DG were conducted by using a specific surface area characterization analyzer (Micromeritics, ASAP2060).

#### 2.3. Electrochemical performance measurements

The electrochemical impedance spectroscopy (EIS) and cyclic voltammetry (CV) of 3DG and NCNT-3DG were conducted using a Potentiostat (Gamry Interface 1000E) using a 3-electrode setup with platinum as a counter electrode, Ag/AgCl as a reference electrode, immersed in a 1 M Na<sub>2</sub>SO<sub>4</sub> aqueous electrolyte. To investigate the Li plating/stripping behavior of the NCNT-3DG current collector, we assembled coin cells with NCNT-3DG as the working electrode and Li foil as the reference and counter electrode. The LSB comprised of a sulfur-loaded 3DG composite (S@3DG) cathode and a Li-plated NCNT-3DG anode (Li@NCT-3DG). The S@3DG composite was prepared by solvothermal synthesis to load sulfur onto 3DG and details have been reported by our group elsewhere [6]. The S@3DG was laser-cut into a circular disc of 11 mm diameter and employed as the cathode which was highly pure and free of any conductive additives or binders. The loading mass of sulfur, obtained by micro-balance weight measurement, was about 2.2 mg cm<sup>-2</sup> for the S@3DG cathode. The NCNT-3DG sample was laser-cut into a circular disc of 12 mm diameter and then lithium-plated resulting a capacity of  $10 \,\mathrm{mAh}\,\mathrm{cm}^{-2}$ , as the final step of forming the anode. All electrochemical tests were carried out in an electrolyte which was a mixture of 1 M lithium bis-trifluoromethanesulfonylimide in 1,3-dioxolane and 1,2dimethoxyethane (1:1 by volume) with 1 wt% LiNO3 additive. A polypropylene film (Celgard 2400) was used as a separator. A galvanostatic charge-discharge instrument (LANHE CT2001A) was employed to characterize the performance of the battery coin cell. The LSBs were galvanostatically charge/discharge cycled between 1.5 and 2.8 V at 0.2C  $(1C = 1675 \text{ mA g}^{-1})$ , and the energy density of the cell was calculated according to Eq. (1)

$$E = \frac{C \times V_n}{m} \tag{1}$$

where C is the capacity,  $V_n$  represents the mid-point voltage (nominal voltage), m is the total mass of cathode and anode.

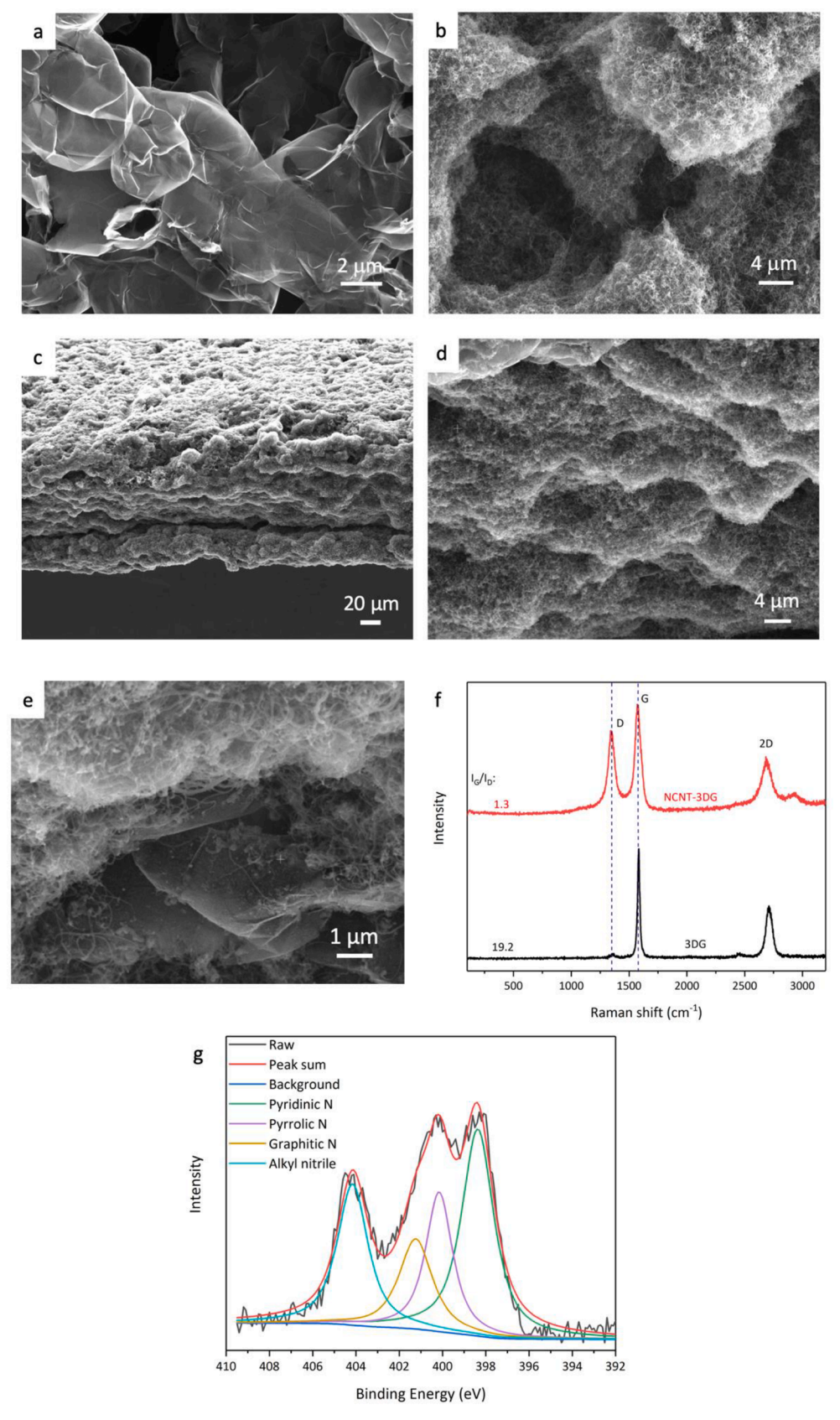


Fig. 1. (a) SEM top view image of 3DG. (b) SEM top view image of NCNT-3DG. (c-e) SEM cross-section image of NCNT-3DG displayed from lower to higher magnification. (f) Raman spectra of 3DG and NCNT-3 DG. (g) High resolution XPS spectrum of N 1 s for NCNT-3DG.

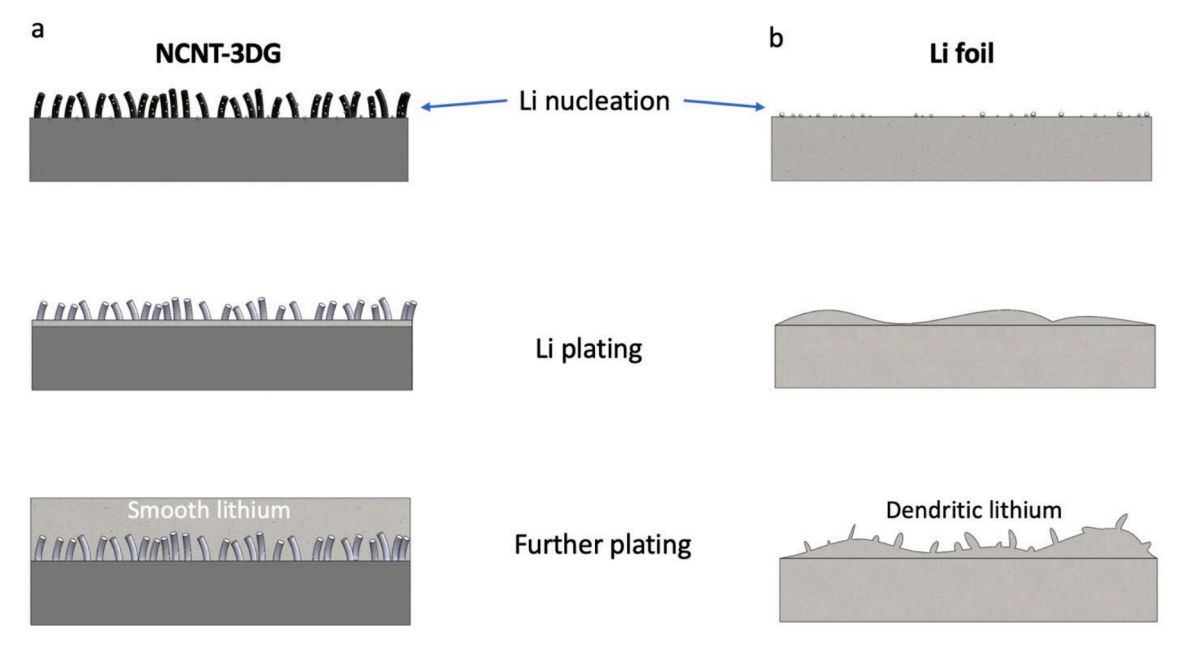


Fig. 2. Schematic illustration of the Li nucleation and plating process on: (a) NCNT-3DG and (b) host-less Li foil.

#### 3. Results and discussion

The NCNT-3DG hybrid host could greatly mitigate the lithium dendrite formation because of its unique structural and chemical properties. The high specific surface area and the intrinsic lithiophilicity of the hybrid can lower the local effective current density thus enabling a uniform Li-ion flux and suppressing Li dendrite growth. The 3DG specifically contributes a robust carbon matrix which helps to minimize the volume changes of Li metal electrodes and at the same time offers a porous scaffold for uniform NCNT growth. The uniformly distributed NCNTs on 3DG act as lithiophilic seeds and guide homogeneous lithium nucleation with small nucleation overpotential. Moreover, the NCNT-3DG hybrid structure showed three-times increase of the surface area compare to 3DG, as illustrated by BET data presented in the Supplementary Information (Fig. S1). This increase is due to the presence of NCNTs grown on 3DG. The obtained grass-like, high surface area NCNT-3DG structures shown in Fig. 1a.b, retain efficient electron and ion pathways, which are essential for uniform lithium deposition. Furthermore, the NCNTs distribute uniformly within the 3DG flake structure as shown clearly in the cross-section view of the SEM images (Fig. 1c-f). The homogeneous growth of NCNTs on the surface and between the graphene layers enhanced the pathways for charge transfer. According to the literature, NCNTs with in situ nitrogen-doping are lithiophilic due to the nitrogen functional groups that have better metallic Li affinity and stronger binding energy with Li atoms than graphene [46–48]. Raman analysis of 3DG and NCNT-3DG was presented in Fig. 1f. The I<sub>G</sub>/I<sub>D</sub> ratio was found to be reduced from 19.2 in pristine 3DG to 1.3 in the NCNT-3DG, suggesting a higher defect concentration in the NCNT-3DG due to nitrogen-induced defects. The XPS analysis in Fig. S3 and Fig. 1g, proved the presence of nitrogen in the NCNTs with concentration of 2.5 at%. The high-resolution N 1 s spectrum of the NCNT-3DG revealed four different N-doping forms including pyridinic N (398.5 eV), pyrrolic N (400.1 eV), graphitic N (402.1 eV), and alkyl nitrile (404.1 eV) [47,57]. Z. Hu et al., have shown that the binding energies between a Li atom and pyridinic or pyrrolic nitrogen are stronger than that in the pristine graphene structures [47]. The alkyl nitrile peak could be attributed to the absorption of the precursor acetonitrile during the CVD process. The uniformly distributed NCNTs on 3DG serve as active sites and guide homogeneous lithium nucleation with small nucleation overpotential. A continuous and homogeneous lithium growth will further suppress dendritic lithium formation.

The nucleation and plating processes of metallic Li on NCNT-3DG and on host-less lithium metal are schematically illustrated in Fig. 2. In the lithium plating process, Li ions migrate toward the surface of the anode. The surface of lithium foil is relatively rough, which leads to a heterogenous and randomly distributed nucleation. The initial heterogeneous nucleation makes the anode surface even rougher, which in the following stage, tends to induce non-uniform lithium plating and growth

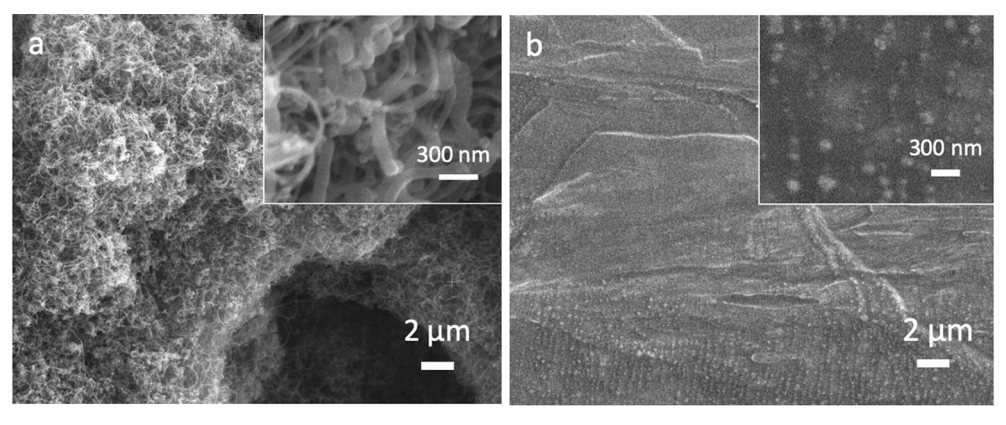
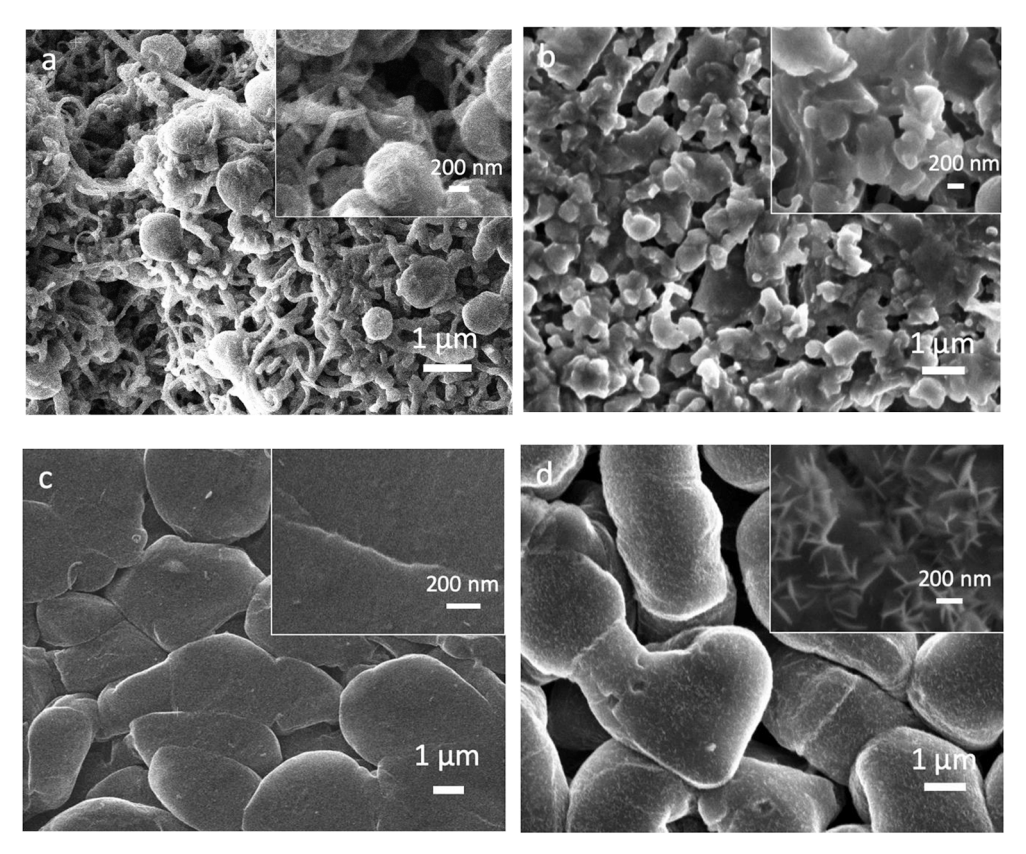


Fig. 3. SEM top view images of (a) NCNT-3DG and (b) lithium foil. Each inset in the images displayed higher magnification.



**Fig. 4.** Top view SEM images of lithium plated samples: (a) 1 mAh cm<sup>-2</sup> plated on NCNT-3DG, (b) 2 mAh cm<sup>-2</sup> plated on NCNT-3DG, (c) 4 mAh cm<sup>-2</sup> plated on NCNT-3DG and (d) 1 mAh cm<sup>-2</sup> plated on lithium chip. Each inset in the images displayed higher magnification.

of lithium dendrites [58]. However, when NCNT-3DG serves as a lithium-plating host, the high surface area and the existence of N-doped groups contribute to a homogeneous lithium nucleation and eventually uniform lithium plating. The high surface area reduces the current density of lithium plating, while N-doped groups improve the lithium affinity of the carbon matrix [50]. The combined effect of these two factors enables a much lower lithium nucleation overpotential, which induces a homogeneous nucleation and uniform lithium plating [47].

The SEM image displayed in Fig. 1a, shows the porous nature of pristine 3DG. Fig. 1b reveals the formation of NCNT on 3DG, thus significantly increasing the specific area of the hybrid material. A closer look at the NCNT-3DG is displayed in Fig. 3a. There, it is obvious that the hybrid perfectly inherits the 3D porous morphology with homogeneous NCNT "grass" sprouted not only outside the surface of the graphene but also inside its pores. Transmission electron microscopy (TEM) of NCNT-3DG presented in Fig. S4 showed that the hybrid materials consisted of transparent graphene flasks and abundant NCNTs with diameter of 20 to 50 nm. The uniform distribution of lithiophilic NCNT on 3DG enables homogeneous nucleation during lithium plating which further utilizes the whole surface area of the 3DG scaffolds. This suppresses the Li dendrite growth and minimizes the volume changes. In contrast to the NCNT-3DG, lithium foil reveals a rough and bulky surface with limited surface area, as displayed in Fig. 3b, showing a top SEM view. Due to the limited surface area and high roughness of the surface, the current density is expected to be greater than that of NCNT-3DG, and the charge distribution may vary, causing heterogenous nucleation.

Fig. 4a–c reveal the evolution of lithium plating on NCNT-3DG tracked by SEM imaging. The plated lithium metal on NCNT-3DG reached capacity of 1, 2 and 4 mAh cm $^{-2}$ , respectively. Initially, with 1 mAh cm $^{-2}$  of lithium plating, an overall thin and uniform lithium decoration can be observed on the NCNTs (Fig. 4a). This indicated that NCNTs served as lithiophilic sites for nucleation, which resulted in a homogeneous lithium plating. The growth of lithium nuclei continued

and evolved into nano-structured, spherical, lithium metal particles with no dendrite formation (Fig. 4a). This spherical metal particle morphology was not observed in 3DG as displayed in the SEM image from the Supplementary Information (Fig. S5), thus indicating the spherical nucleation was induced due to the presence of NCNTs. This is attributed to the electron-rich structure of the graphene, which imposes a negative effect on the Li adsorption <sup>[47]</sup>. The initial pattern of lithium nucleation and growth determines the morphology of on-going lithium plating. With more plated lithium reaching 2 mAh cm<sup>-2</sup> on NCNT-3DG, the spherical metal particles started to merge together into a denser layer (Fig. 4b). Finally, a uniform and dendrite-free lithium film of 4 mAh cm<sup>-2</sup> was plated on the whole surface of the NCNT-3DG (Fig. 4c). On the other hand, lithium foil demonstrated a different morphology of plating even at a capacity of 1 mAh cm<sup>-2</sup> shown in Fig. 4d. Notably, the particle size of lithium there was bulky with bigger gaps between the formed lithium clusters. The surface of these clusters was completely covered with needle-shaped nano-size dendrites (Fig. 4d). In comparison, all NCNT-3DG samples were dendrite-free, even at a high capacity of 10 mAh  ${\rm cm}^{-2}$  employed for lithium plating (Fig. 5).

The morphology evolution of Li-plated NCNT-3DG (Li@NCNT-3DG) and Li-plated Li foil (Li@Li) electrodes after multiple cycles is also investigated by SEM. NCNT-3DG and lithium foil were both plated with an initial capacity of 10 mAh cm<sup>-2</sup>, then the metallic Li was stripped and plated at a current density of 1 mA cm<sup>-2</sup> and a capacity of 1 mAh cm<sup>-2</sup> per cycle for 100 cycles. As indicated in Fig. 5a and b, the Li@NCNT-3DG electrodes remains intact revealing a smooth and crack-free surfaces. No obvious Li agglomerates or dendrites were observed, indicating a homogeneous process of Li stripping and plating. In this case, the volume change was also restrained by the 3D carbon scaffold so the resulted SEI was stable during cycling. In the inset of Fig. 5b, some pitting-type cracks with a diameter below 100 nm, were found on the surface of the lithium metal, which was a result of reasonable volume fluctuation and SEI consumption. On the contrary, the surface of the

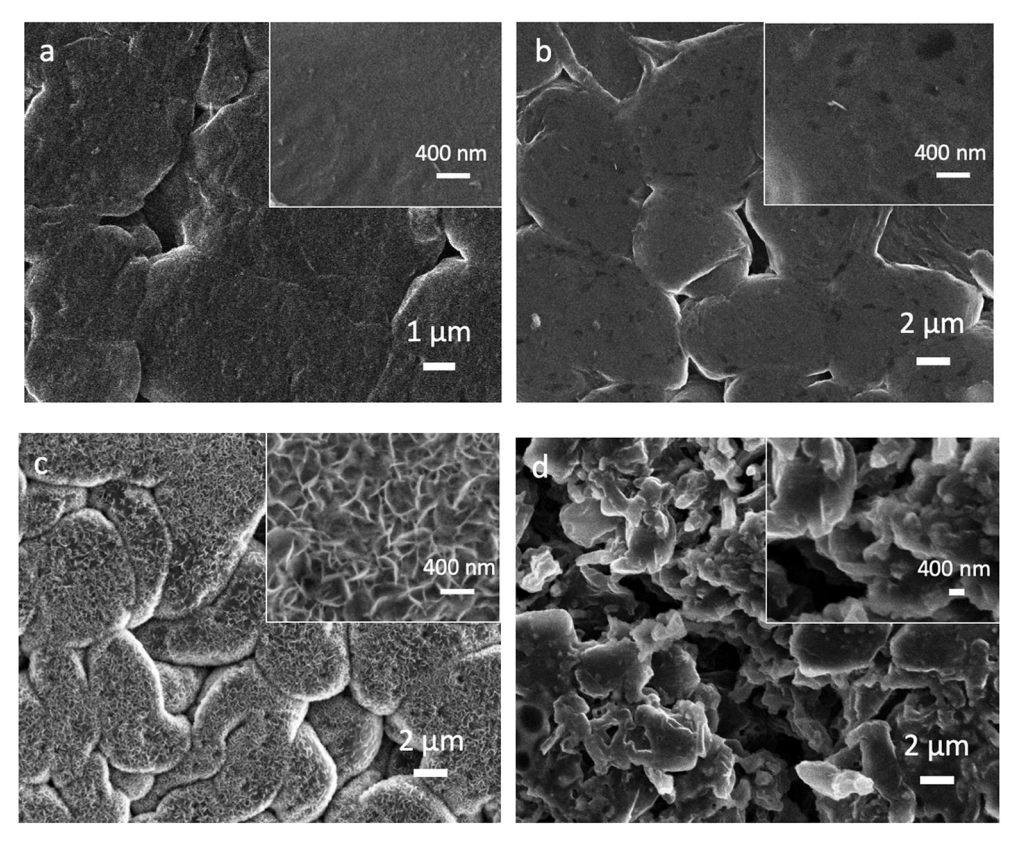


**Fig. 5.** SEM images of: (a) Li@NCNT-3DG before and (b) after 100 cycles of lithium plating and stripping with capacity of 1 mAh cm<sup>-2</sup> per cycle at current density of 1 mA cm<sup>-2</sup>. (c) Li@Li foil before and (d) after 100 cycles of lithium plating and stripping with capacity of 1 mAh cm<sup>-2</sup> per cycle at current density of 1 mA cm<sup>-2</sup>. Each inset in the images displayed higher magnification.

pure Li anode after the initial  $10~\text{mAh}~\text{cm}^{-2}$  plating, revealed plenty of acicular dendrites. The extensive Li dendrite presence led to heterogenous Li stripping and plating and unstable SEI. The SEI cracked due to huge volume fluctuation and fresh Li was exposed and consumed to form new SEI, resulting in more cracks. Finally, as illustrated in Fig. 5d, after 100~cycles, deep and large canyon-shaped cracks on the pure Li anode were observed. The inset image Fig. 5d shows fractures of Li dendrites, indicates that Li dendrites were formed and cracked during multiple cycles.

The incorporation of the NCNT was also evidenced by the improved electrochemical performance of NCNT-3DG over 3DG. The cyclic voltammetry (CV) curves shown in Fig. 6a revealed a 4 time increase in areal capacity of NCNT-3DG over 3DG. This can be explained by the electrochemical impedance spectroscopy (EIS) data in Fig. 6b, which showed a significant drop in the ionic charge transfer resistance (Rct) values from 4.5  $\Omega$  for 3DG to 1.1  $\Omega$  for NCNT-3DG. The grass-type morphology of the CNTs provided easy access for the Li ions and the presence of nitrogen groups increased the specific capacity of the material [59]. The coulombic efficiency (CE) was studied in a half-cell configuration with Li metal as the counter electrode while NCNT-3DG and 3DG were employed as working electrode, respectively. For each cycle, 2 mAh cm<sup>-2</sup> areal capacity of Li plated and then stripped away up to the voltage of 1 V. The average CE of NCNT-3DG electrode was 98.4% for the first 50 cycles at 2 mA cm<sup>-2</sup> current density. Meanwhile, the average CE of 3DG was 92.8% (Fig. 6c). After 100 cycles, the CE of 3DG decreased gradually to 84.5%, while that of NCNT-3DG remained stable even beyond 120 cycles with a high CE of over 98.1%. The galvanostatic cycling performance of Li metal anodes was investigated with a symmetric Li/Li cell configuration [39,40,47]. Lithium foil, NCNT-3DG, as well as 3DG have been employed as working electrode, respectively. They were first plated with a pre-stored capacity of 10 mAh cm<sup>-2</sup> from a counter and reference electrode, which in this case was another Li foil.

The created symmetric cells were then cycled to evaluate the voltage variation during the plating/stripping of lithium at various current densities with a constant areal capacity of 1 mAh cm<sup>-2</sup>. Fig. 6d shows the comparison of voltage profiles in the three types of symmetrical cells (Li@3DG||Li foil, Li@NCNT-3DG||Li foil and Li@Li foil||Li foil) at a current density of 3 mA cm<sup>-2</sup> for 1 mAh cm<sup>-2</sup> areal capacity per cycle. The symmetrical cell of Li@NCNT-3DG exhibits a small overpotential of 21 mV and remarkable long-term cyclability of 1200 cycles (800 h). On the contrary, the symmetrical cell of Li foil shows an unstable voltage profile with a much larger overpotential of about 105 mV, which could be attributed to extensive growth lithium dendrites and corrosion of metallic Li causing an unstable SEI layer [39]. The voltage profile of the 3DG cell is more stable than that of the Li foil cell, while the overpotential of 3DG cell is 51 mV, which is about half of that for the Li foil cell. This could be attributed to the higher surface area of 3DG over Li foil. However, without the NCNTs guiding a uniform lithium plating and stripping, the 3DG cell short-circuited after about 170 cycles. To investigate the voltage profiles in detail, the 15th and 842nd cycles were magnified in the insets of Fig. 6a. The Li@NCNT-3DG symmetrical cell exhibited flat charge-discharge profiles displayed in both insets, with much smaller overpotential.

With the current density increased to 5 mA cm<sup>-2</sup> and 10 mA cm<sup>-2</sup> (Fig. 6e and f), the voltage oscillation of the Li foil cell became too big to support stable Li plating and stripping even at the beginning of the cycling. However, the Li@NCNT-3DG cell still showed small overpotential of about 38 mV and 60 mV at 5 mA cm<sup>-2</sup> and 10 mA cm<sup>-2</sup>, respectively, displaying stable voltage profiles and significantly long lifespan of more than 500 h at current density of 5 mA cm<sup>-2</sup> and 260 h at current density of 10 mA cm<sup>-2</sup>. This data reaches or even surpasses the previously reported results [39,43,60–62]. To evaluate the stability of the Li@NCNT-3DG cell under a large volume change, the areal capacity of each plating and stripping cycle was increased to 3 mAh cm<sup>-2</sup> at

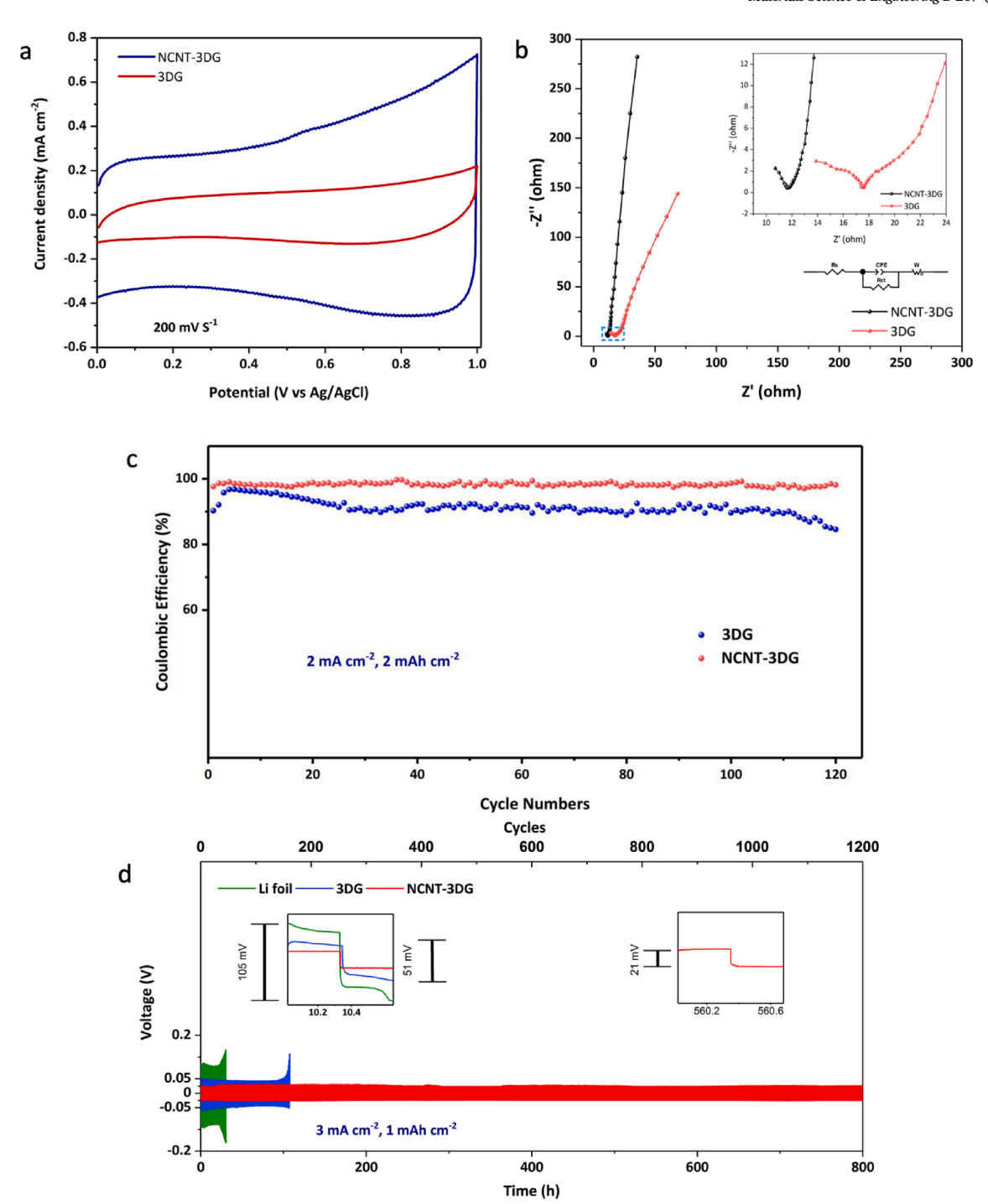


Fig. 6. (a) CV curves of 3DG and NCNT-3DG at a scan rate of 200 mV s<sup>-1</sup>. (b) EIS spectra of 3DG and NCNT-3DG. (c) CE of NCNT-3DG and 3DG with lithium areal capacity of 2 mAh cm<sup>-2</sup> at a current density of 2 mA cm<sup>-2</sup>. (d) Voltage profiles of the conducted Li symmetric test with NCNT-3DG, 3DG and Li foil at current density of 3 mA cm<sup>-2</sup> for areal capacity of 1 mAh cm<sup>-2</sup> per cycle. (e) Voltage profiles of Li symmetric test with NCNT-3DG and Li foil at current density of 5 mA cm<sup>-2</sup> for areal capacity of 1 mAh cm<sup>-2</sup> per cycle. (f) Voltage profiles of Li symmetric test with NCNT-3DG and Li foil at current density of 10 mA cm<sup>-2</sup> for areal capacity of 3 mAh cm<sup>-2</sup> per cycle. (g) Voltage profiles of Li symmetric test with NCNT-3DG and Li foil at current density of 3 mA cm<sup>-2</sup> for areal capacity of 3 mAh cm<sup>-2</sup> per cycle.

current density of 3 mA  $\rm cm^{-2}$ , as shown in Fig. 6g. Under this harsh condition, the voltage profiles of the Li@NCNT-3DG cell were still stable with an overpotential of 30 mV, while the voltage profiles of the Li foil cell were unstable with random voltage oscillations, indicating a sever dendrites formation and corrosion of metallic lithium.

To investigate the potential of the Li@NCNT-3DG anode in a battery system for practical applications, LSBs were assembled with sulfur as the cathode. The electrodes in the batteries were binder-free and the devices

were assembled without any metal current collector. For a reference, half-cell with Li foil as anode, was also constructed. Fig. 7a shows the charge–discharge profiles of the LSBs at 0.2C. Apparently, the Li@NCNT-3DG||S@3DG cell exhibits a much lower voltage polarization than that of Li||S@3DG cell, indicating an enhanced kinetic for Li plating and stripping in Li@NCNT-3DG anode. This is in good agreement with the symmetrical cells discussed above. The Li@NCNT-3DG||S@3DG cell delivers an initial capability at the 3rd cycle, of 1103

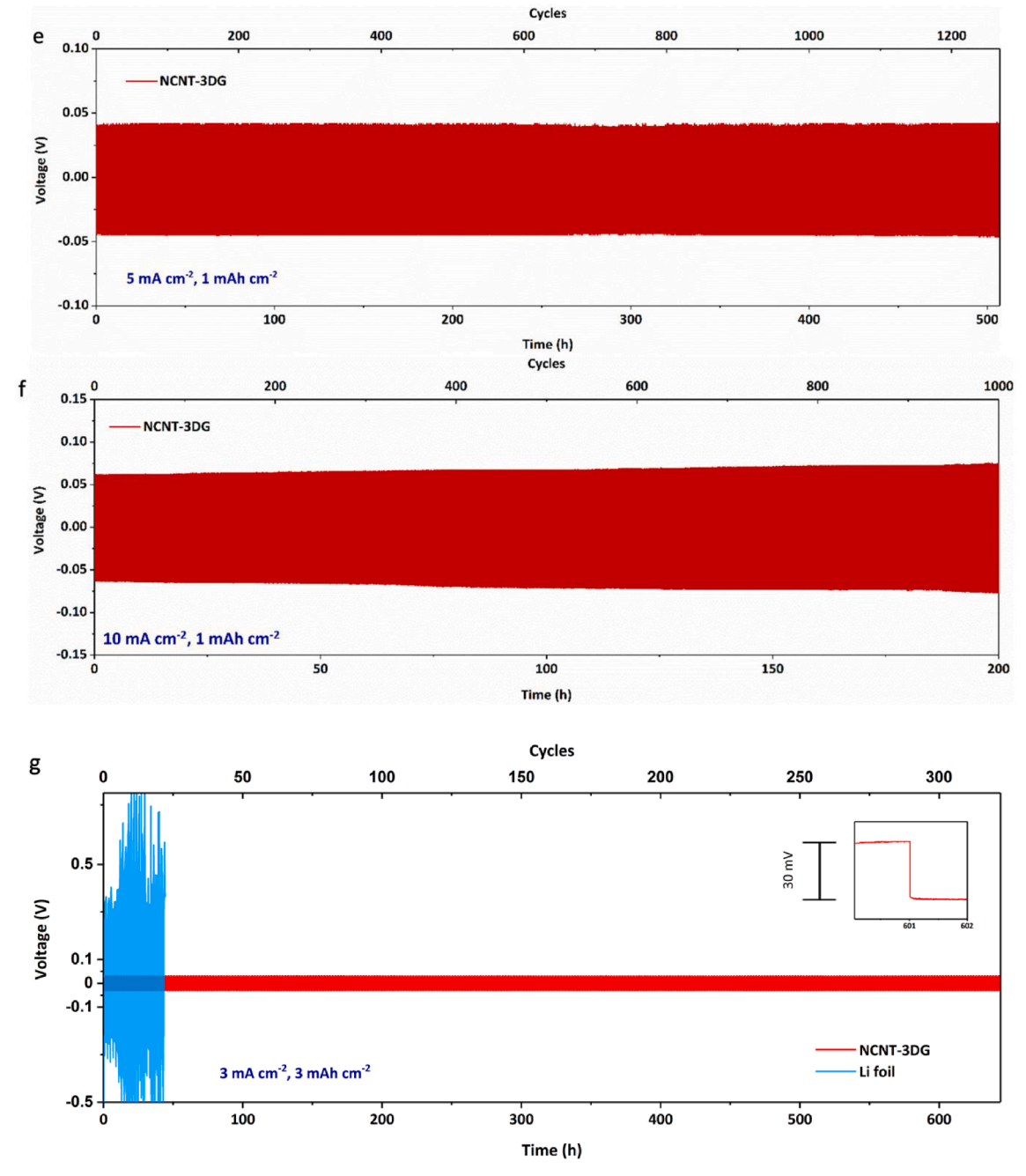


Fig. 6. (continued).

mAh g<sup>-1</sup> and maintains a reversible capacity of 559 mAh g<sup>-1</sup> after 300 cycles. The latter is nearly 51% retention of the initial capacity. Meanwhile, the cell with Li foil anode suffers significant capacity decay from 837 mAh g<sup>-1</sup> to 285 mAh g<sup>-1</sup>, corresponding to only 34% retention of initial capacity. The cell of Li@NCNT-3DG||S@3DG delivers an initial energy density of 770 Wh kg<sup>-1</sup> and 476 Wh kg<sup>-1</sup> after 100 cycles, corresponding to an energy reduction of only 0.48% per cycle. Fig. 7b displays the cycling performance of Li@NCNT-3DG||S@3DG and Li||S@3DG cells at a 0.2C. It is obvious that the cell of Li foil anode exhibits a rapid decay of capacity in the first 20 cycles, which could be ascribed to the unstable SEI in the anode and the severe Li dendrite formation. Remarkably, the CE of Li@NCNT-3DG cell is much more stable and remains nearly constant (99.7%) after the first 20 cycles. It is noted from Fig. 6b that the CE values of Li foil cell fluctuated, exceeding 100% in first 10 cycles, which confirms an unstable SEI and Li dendrite formation in the early cycling stage.

### 4. Conclusions

An advanced NCNT-3DG hybrid structure working as metallic Li host material was synthesized and investigated for applications in Li metal batteries. The unique design of the NCNT-3DG host is featured by its high electrical conductivity, robustness and large interface area. In addition, the hybrid NCNT-3DG structure is synthesized with uniformly distributed CNTs possessing multiple nitrogen functional groups, which offer abundant lithiophilic sites. The latter has a profound effect on guiding a homogeneous lithium nucleation with small nucleation overpotential due to the largely reduced energy barrier. Due to the homogeneous lithium growth, the dendritic lithium formation will be significantly suppressed. As a result, the Li@NCNT-3DG electrodes deliver an excellent cycling stability over 1200 cycles at a high current density of 10 mA cm<sup>-2</sup>. The advantages of Li@NCNT-3DG electrodes ensure an enhanced cycling stability of Li@NCNT-3DG||S@3DG when

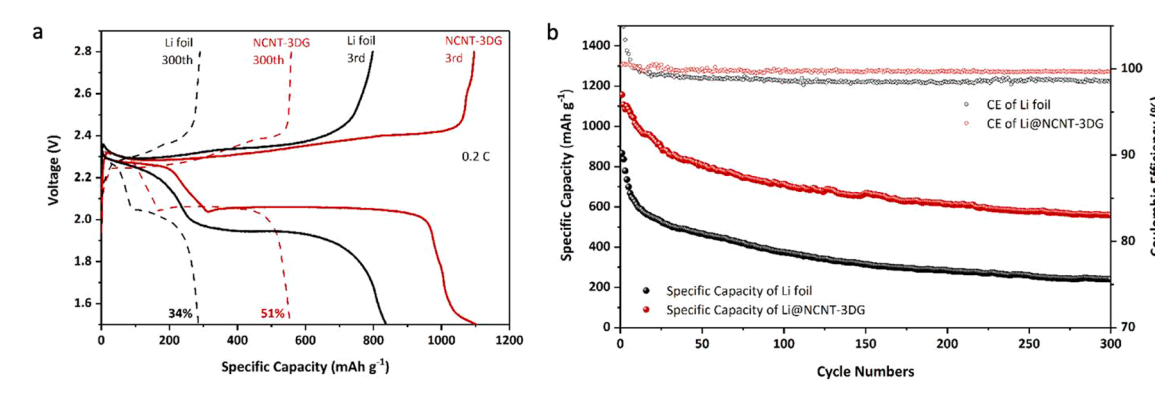


Fig. 7. (a) charge—discharge profiles obtained for the 3rd and 300th cycles, (b) cycling performance at a current density of 0.2C for 300 cycles of Li||S@3DG and Li@NCNT-3DG||S@3DG batteries.

employed in full cells which reached an energy density of 476 Wh  ${\rm kg}^{-1}$  after 100 cycles. We believe that, the proposed lithium 3D host structure enables dendrite-free Li metal anodes and high-cycling stability. This provides new directions for achieving safe performance of Li metal batteries.

#### **Declaration of Competing Interest**

The authors declare that they have no known competing financial interests or personal relationships that could have appeared to influence the work reported in this paper.

#### Acknowledgements

The authors acknowledge the financial support from the NASA [grant NNC16CA17C]; One of the authors (Y. F.) would like to thank NSF for the partial funding through [grant EEC-1404766] and [grant CBET-1706489].

#### Appendix A. Supplementary data

Supplementary data to this article can be found online at https://doi.org/10.1016/j.mseb.2021.115067.

#### References

- [1] M. Armand, J.-M. Tarascon, Nature 451 (2008) 652.
- [2] P.G. Bruce, S.A. Freunberger, L.J. Hardwick, J.-M. Tarascon, Nat. Mater. 11 (2011) 19.
- [3] Y. Wang, R. Chen, T. Chen, H. Lv, G. Zhu, L. Ma, C. Wang, Z. Jin, J. Liu, Energy Storage Mater. 4 (2016) 103.
- [4] Y. Sun, N. Liu, Y. Cui, Nat. Energy 1 (2016) 16071.
- [5] X.-B. Cheng, R. Zhang, C.-Z. Zhao, F. Wei, J.-G. Zhang, Q. Zhang, Adv. Sci. 3 (2016) 1500213.
- [6] Y.Y. Hsieh, L. Zhang, D. DeArmond, S.N. Kanakaraj, P.K. Adusei, N.T. Alvarez, Y. Fang, J. Daum, V. Shanov, Carbon N. Y. 139 (2018) 1093.
- [7] M.S. Whittingham, Science (80) 192 (1976) 1126.
- [8] D. Aurbach, E. Zinigrad, Y. Cohen, H. Teller, Solid State Ionics 148 (2002) 405.
- [9] R.A. Huggins, E. Storage, Lithium (2010) 291.
- [10] D. Aurbach, I. Weissman, A. Schechter, H. Cohen, Langmuir 12 (2002) 3991.
- [11] C.M. López, J.T. Vaughey, D.W. Dees, J. Electrochem. Soc. 156 (2009) A726.
- [12] D. Aurbach, J. Power Sources 89 (2000) 206.
- [13] N. Kamaya, Nat. Mater. 10 (2011) 682.
- [14] H. Wan, G. Peng, X. Yao, J. Yang, P. Cui, X. Xu, Energy Storage Mater. 4 (2016) 59.
- [15] R. Bouchet, S. Maria, R. Meziane, A. Aboulaich, L. Lienafa, J.-P. Bonnet, T.N. T. Phan, D. Bertin, D. Gigmes, D. Devaux, Nat. Mater. 12 (2013) 452.
- [16] E. Peled, J. Electrochem. Soc. 126 (1979) 2047.
- [17] F. Ding, W. Xu, G.L. Graff, J. Zhang, M.L. Sushko, X. Chen, Y. Shao, M. H. Engelhard, Z. Nie, J. Xiao, X. Liu, P.V. Sushko, J. Liu, J.G. Zhang, J. Am. Chem. Soc. 135 (2013) 4450.
- [18] L. Suo, Y.-S. Hu, H. Li, M. Armand, L. Chen, Nat. Commun. 4 (2013) 1481.
- [19] X. Tao, Y. Liu, W. Liu, G. Zhou, J. Zhao, D. Lin, C. Zu, O. Sheng, W. Zhang, H.-W. Lee, Nano Lett. 17 (2017) 2967.
- [20] O. Sheng, C. Jin, J. Luo, H. Yuan, C. Fang, H. Huang, Y. Gan, J. Zhang, Y. Xia, C. Liang, J. Mater. Chem. A 5 (2017) 12934.

- [21] G. Zheng, S.W. Lee, Z. Liang, H.-W. Lee, K. Yan, H. Yao, H. Wang, W. Li, S. Chu, Y. Cui, Nat. Nanotechnol. 9 (2014) 618.
- [22] K. Yan, H.-W. Lee, T. Gao, G. Zheng, H. Yao, H. Wang, Z. Lu, Y. Zhou, Z. Liang, Z. Liu, Nano Lett. 14 (2014) 6016.
- [23] Z. Liang, G. Zheng, C. Liu, N. Liu, W. Li, K. Yan, H. Yao, P.-C. Hsu, S. Chu, Y. Cui, Nano Lett. 15 (2015) 2910.
- [24] J. Luo, C.C. Fang, N.L. Wu, Adv. Energy Mater. 8 (2018) 1.
- [25] K. Liu, A. Pei, H.R. Lee, B. Kong, N. Liu, D. Lin, Y. Liu, C. Liu, P. Chun Hsu, Z. Bao, Y. Cui, J. Am. Chem. Soc. 139 (2017) 4815.
- [26] J. Xie, L. Liao, Y. Gong, Y. Li, F. Shi, A. Pei, J. Sun, R. Zhang, B. Kong, R. Subbaraman, Sci. Adv. 3 (2017) eaao3170.
- [27] N. Li, Y. Yin, C. Yang, Y. Guo, Adv. Mater. 2016 (1853) 28.
- [28] C.-P. Yang, Y.-X. Yin, S.-F. Zhang, N.-W. Li, Y.-G. Guo, Nat. Commun. 6 (2015) 8058.
- [29] D. Lin, Y. Liu, Z. Liang, H.W. Lee, J. Sun, H. Wang, K. Yan, J. Xie, Y. Cui, Nat. Nanotechnol. 11 (2016) 626.
- [30] L.L. Lu, J. Ge, J.N. Yang, S.M. Chen, H. Bin Yao, F. Zhou, S.H. Yu, Nano Lett. 16 (2016) 4431.
- [31] K. Xie, W. Wei, K. Yuan, W. Lu, M. Guo, Z. Li, Q. Song, X. Liu, J.-G. Wang, C. Shen, ACS Appl Mater. Interfaces 8 (2016) 26091.
- [32] Z. Liang, D. Lin, J. Zhao, Z. Lu, Y. Liu, C. Liu, Y. Lu, H. Wang, K. Yan, X. Tao, Proc. Natl. Acad. Sci. 113 (2016) 2862.
- [33] Y. Liu, D. Lin, Z. Liang, J. Zhao, K. Yan, Y. Cui, Nat. Commun. 7 (2016) 10992.
- [34] Q. Yun, Y.-B. He, W. Lv, Y. Zhao, B. Li, F. Kang, Q.-H. Yang, Adv. Mater. 28 (2016) 6932.
- [35] Y. Zhang, W. Luo, C. Wang, Y. Li, C. Chen, J. Song, J. Dai, E.M. Hitz, S. Xu, C. Yang, Proc. Natl. Acad. Sci. 114 (2017) 3584.
- [36] Y. Zhang, B. Liu, E. Hitz, W. Luo, Y. Yao, Y. Li, J. Dai, C. Chen, Y. Wang, C. Yang, H. Li, L. Hu, Nano Res. 10 (2017) 1356.
- [37] X.B. Cheng, R. Zhang, C.Z. Zhao, Q. Zhang, Chem. Rev. 117 (2017) 10403.
- [38] W. Xu, J. Wang, F. Ding, X. Chen, E. Nasybulin, Y. Zhang, J.G. Zhang, Energy Environ. Sci. 7 (2014) 513.
- [39] L. Liu, Y.-X. Yin, J.-Y. Li, S.-H. Wang, Y.-G. Guo, L.-J. Wan, Adv. Mater. 30 (2018) 1706216.
- [40] S. Liu, A. Wang, Q. Li, J. Wu, K. Chiou, J. Huang, J. Luo, Joule 2 (2018) 184.
- [41] Z. Hu, Z. Li, Z. Xia, T. Jiang, G. Wang, J. Sun, Energy Storage Mater. (2018) 1.
- [42] Y. Zhao, Q. Sun, X. Li, C. Wang, Y. Sun, K.R. Adair, R. Li, X. Sun, Nano Energy 43 (2018) 368.
- [43] T.-T. Zuo, X.-W. Wu, C.-P. Yang, Y.-X. Yin, H. Ye, N.-W. Li, Y.-G. Guo, Adv. Mater. 29 (2017) 1700389.
- [44] J. Lang, Y. Jin, X. Luo, Z. Liu, J. Song, Y. Long, L. Qi, M. Fang, Z. Li, H. Wu, J. Mater. Chem. A 5 (2017) 19168.
- [45] Y. Tang, J. Sha, N. Wang, R. Zhang, L. Ma, C. Shi, E. Liu, N. Zhao, Carbon N. Y. 158 (2020) 536.
- [46] K. Yan, Z. Lu, H.W. Lee, F. Xiong, P.C. Hsu, Y. Li, J. Zhao, S. Chu, Y. Cui, Nat. Energy (2016) 1, https://doi.org/10.1038/NENERGY.2016.10.
- [47] R. Zhang, X.R. Chen, X. Chen, X.B. Cheng, X.Q. Zhang, C. Yan, Q. Zhang, Angew. Chemie - Int. Ed. 56 (2017) 7764.
- [48] H. Zhang, X. Liao, Y. Guan, Y. Xiang, M. Li, W. Zhang, X. Zhu, H. Ming, L. Lu, J. Qiu, Y. Huang, G. Cao, Y. Yang, L. Mai, Y. Zhao, H. Zhang, Nat. Commun. 9 (2018) 1.
- [49] Y. Yu, W. Huang, X. Song, W. Wang, Z. Hou, X. Zhao, K. Deng, H. Ju, Y. Sun, Y. Zhao, Y.-C. Lu, Z. Quan, Electrochim. Acta 294 (2019) 413.
- [50] Z. Wang, G. Huang, K. Watanabe, F. Zhang, H. Kashani, J. Han, M. Chen, Adv. Mater. 31 (2018) 1805334.
- [51] Y. Xu, A. Sreekumar, P. Paul, R.M.L. Harks, D.C. Hermes, Energy Storage Mater. 12 (2018) 69.
- (2018) 69. [52] S. Chi, Y. Liu, W. Song, L. Fan, Q. Zhang, Adv. Funct. Mater. 27 (2017) 1700348.
- [53] Y. An, Y. Tian, H. Wei, B. Xi, S. Xiong, J. Feng, Y. Qian, Adv. Funct. Mater. 1908721 (2019) 1.
- [54] J. Collins, J. P. de Souza, M. Hopstaken, J. A. Ott, S. W. Bedell, D. K. Sadana, iScience 2020, 23, 101586.
- [55] Y.Y. Hsieh, Y. Fang, J. Daum, S.N. Kanakaraj, G. Zhang, S. Mishra, S. Gbordzoe, V. Shanov, Carbon N. Y. (2019), https://doi.org/10.1016/j.carbon.2019.01.055.

- [56] L. Zhang, D. DeArmond, N.T. Alvarez, R. Malik, N. Oslin, C. McConnell, P. K. Adusei, Y.-Y. Hsieh, V. Shanov, Small 13 (2017) 1603114.
- [57] R.J.J. Jansen, H. van Bekkum, Carbon N. Y. 33 (1995) 1021.
- [58] K.N. Wood, E. Kazyak, A.F. Chadwick, K.H. Chen, J.G. Zhang, K. Thornton, N. P. Dasgupta, ACS Cent Sci. 2 (2016) 790.
- [59] B. You, L. Wang, L. Yao, J. Yang, Chem. Commun. 49 (2013) 5016.
- [60] W. Deng, W. Zhu, X. Zhou, X. Peng, Z. Liu, ACS Appl. Mater. Interfaces 10 (2018) 20387.
- [61] R. Zhang, X. Chen, R. Zhang, X. Chen, X. Shen, X. Zhang, X. Chen, X. Cheng, Joule (2018) 1.
- [62] J. Cui, S. Yao, M. Ihsan-Ul-Haq, J. Wu, J.K. Kim, Adv. Energy Mater. 9 (2019) 1.
  [63] K. Dasgupta, M. Khosravifar, S. Sawant, P.K. Adusei, S.N Kanakaraj, J. Kasik, V. Shanov, C 6 (2020) 40.